

MARS: a Multimodal Alignment and Ranking System for Few-Shot Segmentation

Nico Catalano*
nico.catalano@polimi.it

Paolo Pertino*
paolo.pertino@polimi.it

Stefano Samele*
stefano.samele@polimi.it

Matteo Matteucci
matteo.matteucci@polimi.it

Politecnico di Milano

*Equal contribution

arXiv:2504.07942v2 [cs.CV] 21 Jul 2025

Abstract

Few Shot Segmentation aims to segment novel object classes given only a handful of labeled examples, enabling rapid adaptation with minimal supervision. Current literature crucially lacks a selection method that goes beyond visual similarity between the query and example images, leading to suboptimal predictions. We present MARS, a plug-and-play ranking system that leverages multimodal cues to filter and merge mask proposals robustly. Starting from a set of mask predictions for a single query image, we score, filter, and merge them to improve results. Proposals are evaluated using multimodal scores computed at local and global levels. Extensive experiments on COCO-20ⁱ, Pascal-5ⁱ, LVIS-92ⁱ, and FSS-1000 demonstrate that integrating all four scoring components is crucial for robust ranking, validating our contribution. As MARS can be effortlessly integrated with various mask proposal systems, we deploy it across a wide range of top-performer methods and achieve new state-of-the-art results on multiple existing benchmarks. Code will be available upon acceptance.

1 Introduction

Extending the capabilities of traditional segmentation models to new classes often requires retraining with large annotated datasets. This data-collecting process becomes especially prohibitive in domains such as medical imaging, industrial applications, or satellite imagery. Few Shot Segmentation (FSS) [21, 20] offers a promising alternative by reusing knowledge acquired from diverse classes and tasks, enabling models to adapt to new classes with only a handful of annotated examples. Despite the recent advancements in the field, top-performing methods often fail because of visual dissimilarity between the provided example and the query image. We contribute to this research field by presenting a Multimodal Alignment and Ranking System (MARS). The method is capable of scoring, filtering, and merging mask proposals from any existing

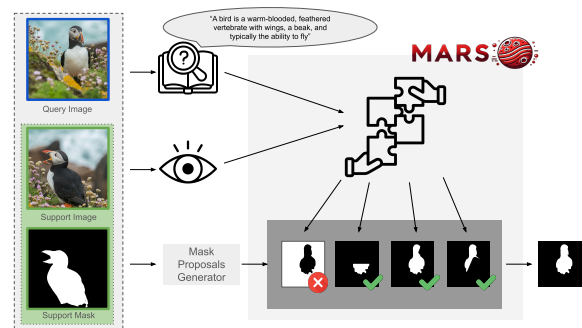


Figure 1: Model Overview: The query image and support set undergo visual and textual analysis. Combining different modalities, we select candidates from the mask proposals generator. The selected ones are merged to form the final prediction.

FSS method, effectively boosting the performance of several algorithms across different benchmark datasets. A high-level depiction of the model is presented in Figure 1. We achieve this goal leveraging four distinct scores: i) *Local Conceptual Score (LC)*, ii) *Global Conceptual Score (GC)*, iii) *Local Visual Score (LV)*, and iv) *Global Visual Score (GV)*. *Visual* scores are derived from direct correspondences between the support and query images, following established approaches [13, 29]. However, we conjecture that visual cues alone may prove insufficient in challenging scenarios characterized by intraclass variation, occlusions, challenging camera angles, and cut-offs. To overcome these limitations, we introduce two *conceptual* scores based on the inferred class name and definition of the subject of interest, able to establish a higher-order semantic similarity. Summarizing, our work makes the following contributions:

- **Multimodal Approach:** We introduce a novel multimodal framework for FSS that leverages both visual and conceptual cues.
- **Scoring System:** We propose a plug-and-play ranking with four scores: three novel and one EMD based.

- **State-of-the-Art Performance:** Extensive experiments on benchmark datasets demonstrate that our approach establishes new state-of-the-art results.

2 Related Works

Traditional FSS [31, 4, 25, 14, 16, 8] approaches typically rely on pre-trained backbone networks, such as ResNet [7, 28], VGG [22] or DINO-trained ViT [5, 2, 18], to extract rich feature representations from both support and query images. These features are then processed by trainable modules that compare and match them to predict the query mask. Owing to their tailored design and dedicated training for few-shot scenarios, such methods are often referred to as specialist models.

In contrast, recent developments leverage foundational models like the Segment Anything Model (SAM) [9]. SAM is capable of segmenting any object when provided with various types of prompts (e.g., points, coarse masks, bounding boxes), yet it does not inherently offer semantic labeling. Consequently, adapting SAM for FSS shifts the emphasis from direct feature matching to an effective prompting strategy. This often requires identifying candidate points by comparing features from the support examples to those in the query images, using these points to generate prompts that guide SAM in producing candidate mask proposals [30, 23, 13, 27, 29].

Several innovative models have emerged along these lines. For instance, PerSAM [30] introduces a training-free personalization approach for SAM. It uses one-shot data, a reference image and a rough mask of the desired concept, to generate a location confidence map that identifies the target object. Based on the confidence scores, two points are selected as positive and negative priors, which are then encoded as prompt tokens for SAM’s decoder to produce the segmentation.

Similarly, VRP-SAM [23] incorporates a Visual Reference Prompt (VRP) encoder. Differently from SAM original prompt encoder, this one leverages both a support image with annotations and a query image to create prompt embeddings. It is composed of a Feature Augmenter, which embeds both images into a shared latent space and extracts prototype features from the support image, and a Prompt Generator that refines these features through attention mechanisms interacting with the query representation. The resulting semantic reference prompt embeddings replace traditional prompts, directly guiding SAM’s mask decoder.

Among the newer methods, Matcher [13] and GF-SAM [29] stand out. Matcher is designed for FSS by embedding both support and query images. Exploiting the natural correspondence between spatial locations in the feature volume and image patches, Matcher computes a similarity matrix to identify highly similar regions. High-similarity points are selected as prompts for SAM, and the subsequent mask predictions are aggregated to generate the final segmentation output.

GF-SAM takes a graph-based approach to prompt selection and ambiguity resolution. It constructs a directed

graph where nodes represent point prompts and edges capture the relationships based on mask coverage. By partitioning this graph into weakly connected components, GF-SAM clusters candidate points and corresponding masks.

Recent advancements also involve SegGPT [27], a trained-from-scratch segmentation model that unifies multiple tasks under an in-context learning framework. It processes all segmentation data in a standardized image format and employs an in-context coloring strategy, where random color mappings guide learning. This approach enables SegGPT to generalize across various segmentation tasks, including object, part, contour, and text segmentation in both images and videos.

3 Method

The FSS setting is defined by a semantic class l , a support set consists of k samples $S(l) = \{(I^i, M_l^i)\}_{i=1}^k$, where I^i is an RGB image, and a binary mask M_l^i that highlights the pixels corresponding to class l in I^i . The goal for a FSS model f_θ is to predict the segmentation mask \hat{M}_q for the query image I_q :

$$\hat{M}_q = f_\theta(I_q, S(l)). \quad (1)$$

Our pipeline works with a set of mask proposals $M_P(I_q, S(l))$ generated by FSS models. We refine these predictions by incorporating both visual and textual alignment. The process consists of five key steps, all leveraging pre-trained models:

1. **Textual Information Retrieval Module:** We first use ViP-LLaVA [1] and WordNet [15] to extract a class name c and a textual description t from the support set images.
2. **Visual-Text Alignment Module:** The query image I_q is encoded using the CLIP [19] image encoder, while the class name c is processed through the CLIP text encoder. We then compute the *Refined Text Alignment* quantity, which contributes to the computation of the LC score.
3. **AlphaClip Module:** The dot product between AlphaCLIP [24] embeddings of $\{c, t\}$, and I_q is used as core quantity to compute GC score.
4. **Visual-Visual Alignment Module** Embedding features from the query image I_q and support set $S(l)$ are extracted using a ViT Model [18]. These features produce two key outputs: a *Refined Visual Alignment* and a *Cost Matrix*, which contribute to computing the LV and GV scores, respectively.
5. **Filtering-Merging Module:** All the scores are always computed with respect to a mask proposal $m_i \in M_P(I_q, S(l))$. The final score is computed as a simple average of the four. A final threshold-based filtering and merging strategy outputs the best mask.

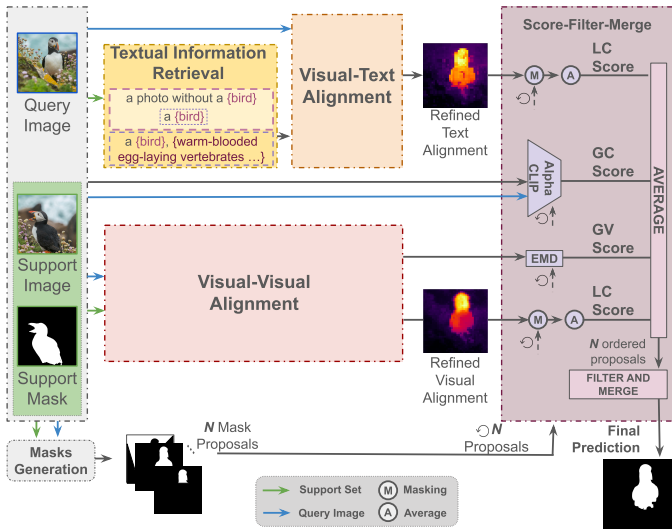


Figure 2: Overview of the proposed MARS model. The diagram illustrates the key components and interactions within the framework. We highlight the Textual Information Retrieval, Visual-Text Alignment, Visual-Visual Alignment, and the Score-Filter-Merge Modules in different colors.

A complete overview of our pipeline is shown in Fig. 2, with complete details provided in the following sections and Fig. 3.

3.1 Textual Information Retrieval Module

In the FSS problem the model can leverage solely the information available in the support set to guide the segmentation of a novel class. To adhere to this principle and ensure continuity with the FSS literature, we infer all necessary textual information directly from the support image rather than using externally provided class names.

We employ pretrained ViP-LLaVA to extract the class name from the support image by overlaying a red contour on the target object and applying a 50% zoom (as detailed in Section 6.2 of Supplemental Material), balancing emphasis on object detail with contextual information. In N -shot settings, where the support set consists of N image-mask pairs, ViP-LLaVA is queried for each image individually, and a majority voting scheme is applied to select the most frequent class name for subsequent processing. This solution enables us to quickly extend all the modules based on textual information to the N -shot scenario.

In addition to the class name, we derive a broader textual description of the entity by leveraging WordNet. The extracted class name is used to query WordNet, which returns a set of candidate synsets. If a single synset is returned, its definition is directly adopted as the object’s description. In cases where multiple synsets are retrieved, indicating potential ambiguity, we prompt ViP-LLaVA (using the same configuration as for class name extraction) to generate a description of the entity.

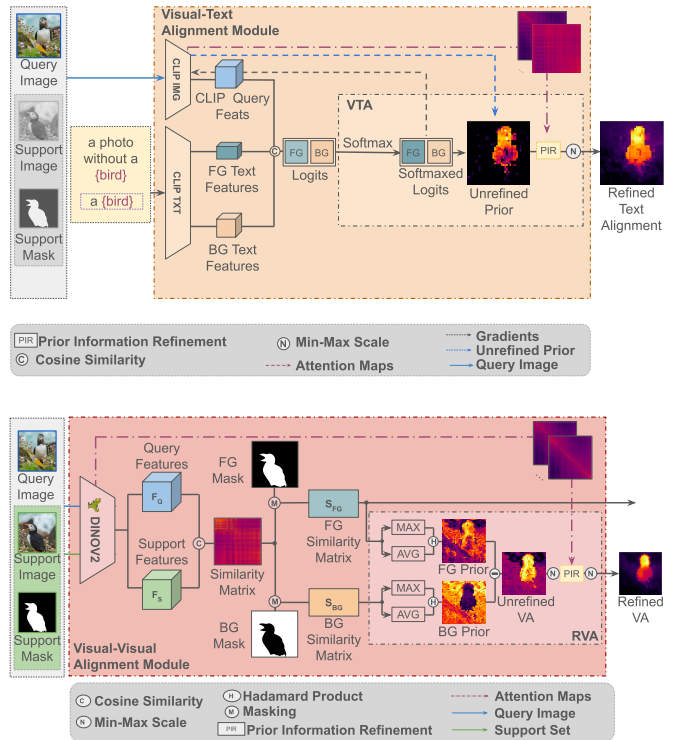


Figure 3: Detailed view of the Visual-Text and Visual-Visual Alignment modules. The **Visual-Text Alignment** module (top) extracts features from the query image using CLIP and aligns them with foreground and background textual features to generate the Softmax-GradCAM map, referred to as the unrefined text prior. This prior is subsequently refined through the PIR module, adapted from [26]. The **Visual-Visual Alignment** module (bottom) computes similarity between query and support features using cosine similarity. Foreground and background priors are obtained by aggregating the respective similarity matrices, and the resulting visual prior is refined using the PIR module for downstream processing.

The VLM-generated description is then compared with the candidate definitions from WordNet, and the definition with the maximum words overlap is selected as the final class description. If no overlap is found between the VLM-generated description and any of the WordNet definitions, an empty description is used. Note that the description produced by ViP-LLaVA is used solely for matching purposes, as it may incorporate visual context specific to the support image.

The extracted textual information is used in two ways in the remainder of the pipeline. The Visual-Text Alignment module employs the class name to determine local conceptual information that enables the computation of the *Local Conceptual Score* (LC). The AlphaClip Module uses the derived description together with the class name to produce the *Global Conceptual Score* (GC).

3.2 Visual-Text Alignment Module

This module generates a Refined Text Alignment, a saliency map that highlights regions in the query image where the subject described by the class name is likely located. Leveraging the visual-text alignment capabilities of a pre-trained CLIP model [19], the module first produces a coarse Text Alignment. Then it refines it through the PI-CLIP [26] Prior Information Refinement (PIR) process followed by min-max normalization. The final Refined Text Alignment is later used to compute the Local Conceptual Score by being multiplied element-wise with each binary mask proposal, with the resulting non-zero values averaged to yield a single score for ranking. A depiction of the model is provided in the upper part of Fig. 3.

The process inspired by [26, 11] begins by encoding the query image using the CLIP vision encoder. Discarding the classification token, we obtain the visual query features $F_q^v \in \mathbb{R}^{d \times (hw)}$, where h, w are the embedding spatial dimensions and d the number of features. A global query token is then computed by applying average pooling over the spatial dimensions:

$$v_q = \frac{1}{hw} \sum_{i=1}^{hw} F_q^v(i), \quad v_q \in \mathbb{R}^{d \times 1}. \quad (2)$$

In parallel, and using the class name from the Textual Information Retrieval Module, two simple text prompts, “a {predicted-class-name}”, and “a photo without {predicted-class-name}”, are embedded by the CLIP text encoder to obtain text features F_{FG}^t and F_{BG}^t , which focus on the subject (foreground) and the background, respectively. Unlike PI-CLIP, which incorporates the names of all objects present in the query image using ground truth annotations, MARS employs only two prompts derived through the Textual Information Retrieval Module. The similarity between the query token and these text features is then computed using a softmax function with a temperature parameter τ (set to 0.01, as in PI-CLIP and [11]):

$$SM_{FG}, SM_{BG} = \text{softmax} \left(\frac{v_q^T F_{FG}^t}{\|v_q\| \cdot \|F_{FG}^t\| \tau}, \frac{v_q^T F_{BG}^t}{\|v_q\| \cdot \|F_{BG}^t\| \tau} \right). \quad (3)$$

Using SM_{FG} , gradients with respect to each feature map are computed to obtain weights:

$$w_m = \frac{1}{hw} \sum_{i,j} \frac{\partial SM_{FG}}{\partial F_q^m(i,j)}, \quad (4)$$

where (i, j) denote spatial positions in the m -th feature map. The initial Text Alignment (TA) is then calculated as:

$$TA = \text{ReLU} \left(\sum_m w_m F_q^m \right). \quad (5)$$

To enhance spatial coherence and semantic precision of the text prior, we employ the Prior Information Refinement (PIR) module [26], which aggregates and normalizes the self-attention map A from the CLIP vision encoder.

A binary box mask B is then derived from TA via thresholding (with a threshold of 0.4, following [26, 12]). The Refined Text Alignment (RTA) is computed as:

$$RTA = B \odot \text{PIR}(A) \cdot TA, \quad (6)$$

where \odot represents the Hadamard product.

The resulting RTA is further processed using min-max normalization. For each mask proposal $m_i \in M_P(I_q, S(l))$, where $M_P(I_q, S(l))$ is the set of all mask proposals for query image I_q , we compute the *Local Conceptual Score* by taking the element-wise multiplication between RTA and m_i , after the support mask is max-pooled to the patch-feature spatial dimension of CLIP features. We then average the resulting values over all non-zero spatial positions. Finally, we also add a coverage term, which accounts for the ratio between the area of the mask proposal m_i and the area of the mask obtained by merging all the masks in $M_P(I_q, S(l))$.

$$\text{Cov}(m_i) = \frac{\text{Area}(m_i)}{\text{Area}(\bigvee_{i=1}^N m_i)}$$

where $\text{Area}(\cdot)$ computes the area of the binary mask passed as an argument by counting its nonzero elements, and $\bigvee_{i=1}^N m_i$ represents the logical OR. The final formulation of the *Local Conceptual* scores is as follows:

$$LC(m_i) = \frac{\alpha}{\|m_i\|_1} \sum_{m_i(x,y) \neq 0} RTA(x,y) m_i(x,y) + (1 - \alpha) \text{Cov}(m_i) \quad (7)$$

where $\|m_i\|_1$ denotes the sum of all elements in m_i , and $\alpha = 0.85$ a fixed weight. This score quantifies the alignment between the salient regions indicated by the textual prior and the mask proposal.

3.3 AlphaCLIP Module

In scenarios where several visual challenges lead to significant differences between the support and query images, purely visual approaches may fail to align the object of interest accurately. To address this, we generate a broad class description using WordNet from the class name predicted by ViP-LLaVA. This comprehensive textual description is then used to assess how well each mask proposal aligns with the expected semantics through the AlphaCLIP module [24], an enhanced version of the CLIP model that enables precise focus on specific regions within an image highlighted by a mask.

Given a query image I_q , a set of N mask proposals $M_P(I_q, S(l))$, and a single class name $c(m_i)$ and textual description $t(m_i)$, obtained by the Textual Information Retrieval module, a pre-trained AlphaCLIP computes an alignment score for each mask proposal relative to (c, t) . First, the text encoder f_{txt} produces an embedding:

$$\mathbf{e}_{txt} = f_{txt}(c, t). \quad (8)$$

In this case, the text processed by AlphaCLIP is constructed by simply concatenating the class name $\$c\$$ with

its corresponding definition $\$t\$, resulting in the text: “a {c}, {t}”. For each mask proposal m_i , the image encoder f_{img} processes the query image I_q together with m_i to generate an embedding:$

$$\mathbf{e}_{img}(m_i) = f_{img}(I_q, m_i), \quad i = 1, \dots, N. \quad (9)$$

Both embeddings are normalized to have unit norm:

$$\hat{\mathbf{e}}_{txt}(m_i) = \frac{\mathbf{e}_{txt}}{\|\mathbf{e}_{txt}\|_2}, \quad \hat{\mathbf{e}}_{img}(m_i) = \frac{\mathbf{e}_{img}^i}{\|\mathbf{e}_{img}^i\|_2}. \quad (10)$$

The alignment score for each mask proposal is computed as the cosine similarity between the corresponding normalized image and text embeddings and then rescaled to the range $[0, 1]$:

$$GC(m_i) = \frac{\hat{\mathbf{e}}_{img}(m_i) \cdot \hat{\mathbf{e}}_{txt}(m_i) + 1}{2}. \quad (11)$$

This yields the final *Global Conceptual Score* for each mask proposal. As the alignment is computed between the image embedding restricted by the mask proposal and the text embedding, this score has a pure global nature with respect to the region of interest highlighted by the support set.

3.4 Visual-Visual Alignment Module

This module leverages solely visual information to compute both the *Global Visual Score* and the *Local Visual Score* for each mask proposal. It aims to capture holistic and localized visual similarities between the support and query images.

Initially, patch features are extracted from the support and query images using a pre-trained DinoV2 ViT-Large using four registers [3], yielding feature maps F_S and F_Q , respectively. A similarity matrix S is then computed by comparing these features using a dot product. In the case of N support images, we stack the relative features along one dimension. This matrix, whose rows correspond to support patches and columns to query patches, is used to derive the foreground and background similarity matrices by selectively retaining rows. Specifically, the support mask is max-pooled to the patch-feature spatial dimension of the encoder. Only the rows corresponding to the regions covered by the support mask (or its complement) are preserved to form the foreground similarity matrix S_{FG} and the background similarity matrix S_{BG} , respectively. We then compute the cost matrix C_{FG} as:

$$C_{FG} = \frac{1 - S_{FG}}{2}. \quad (12)$$

The *Global Visual Score* for a mask proposal m_i is then computed as:

$$GV(m_i) = 1 - \text{EMD}(C_{FG}, M_S, m_i), \quad (13)$$

where EMD denotes the Earth Mover’s Distance, M_S is the support mask, and m_i is a mask proposal. Because of the nature of the EMD, the proposed GC score considers

both the magnitude of differences and the spatial relationships between the embedding distributions; it refers thus to the image part highlighted by the support mask as a whole.

The *Local Visual Score* is based on a Refined Visual Alignment (RVA), which is derived from the combination of S_{FG} and S_{BG} as follows. For both S_{FG} and S_{BG} , two preliminary saliency maps are computed using average and max aggregation on S_{FG} and S_{BG} column-wise, yielding to:

$$S_{FG}^{avg}, \quad S_{FG}^{max}, \quad S_{BG}^{avg}, \quad S_{BG}^{max}. \quad (14)$$

Following the findings in [29], the mean foreground similarity map captures global similarity to the reference object. Still, it may blur internal details, while the max foreground similarity map emphasizes highly similar regions, improving recall but increasing noise. To balance these effects, their Hadamard product is computed, obtaining the mixed similarity maps:

$$S_{FG}^{mix} = S_{FG}^{max} \odot S_{FG}^{avg}, \quad S_{BG}^{mix} = S_{BG}^{max} \odot S_{BG}^{avg}. \quad (15)$$

Similarly to what is done through the softmax function in Section 3.2, we propose a background suppression mechanism in the visual domain. Specifically, the foreground similarity map is further polished by subtracting the background similarity map, effectively eliminating any residual noise and ensuring that misleading background spikes do not interfere with the subsequent scoring stage. Following these insights, the *RVA* is computed as:

$$RVA' = S_{FG}^{mix} - S_{BG}^{mix}, \quad (16)$$

RVA' is subsequently min-max normalized and processed through the PIR module, using all the attention maps A_{DINO} extracted from DINOv2:

$$RVA = \text{PIR}(RVA', A_{DINO}). \quad (17)$$

Again a min-max normalized *RVA* can be used to compute the score for each mask proposal m_i , adding the coverage:

$$LV(m_i) = \frac{\alpha}{\|m_i\|_1} \sum_{m_i(x,y) \neq 0} RVA(x,y) m_i(x,y) + (1 - \alpha) \text{Cov}(m_i), \quad (18)$$

where $\|m_i\|_1$ denotes the sum of all elements in the mask, effectively normalizing the score by the area of the mask, and $\alpha = 0.85$.

The design of the two scores ensures that both global alignment and localized feature correspondences are effectively captured, thereby complementing the textual cues provided by the other modules in our pipeline. A depiction of the model is provided in the bottom part of Fig. 3.

3.5 Filtering-Merging Module

Each mask proposal $m_i \in M_P(I_q, S(l))$, where $M_P(I_q, S(l))$ is the set of all mask proposals related to query image I_q , is evaluated using four distinct scores:

$LC(m_i)$, $GC(m_i)$, $LV(m_i)$, $GV(m_i)$. To derive an overall confidence measure for each proposal, we compute the MARS score as the average of these four scores:

$$\text{MARS}(m_i) = \frac{1}{4} \left(LC(m_i) + GC(m_i) + LV(m_i) + GV(m_i) \right). \quad (19)$$

We then apply a two-step filtering procedure. First, a static threshold $th_s = 0.55$ filters out lower-confidence proposals.

$$M_P^{th_s}(I_q) = \{m_i \in M_P(I_q, S(l)) \mid \text{MARS}(m_i) \geq th_s\}. \quad (20)$$

if $M_P^{th_s}(I_q) = \emptyset$, we apply a dynamic threshold $th_d = 0.95$ to $M_P(I_q, S(l))$:

$$M_P^{th_d}(I_q) = \{m_i \in M_P(I_q, S(l)) \mid \text{MARS}(m_i) \geq \max_{m_j \in M_P(I_q, S(l))} \text{MARS}(m_j) * th_d\}. \quad (21)$$

The fixed threshold, the dynamic threshold, and the coverage weight are the only hyperparameters introduced by the method. Finally, the predicted segmentation mask \hat{M}_q is obtained by performing a logical OR operation over the filtered proposals:

$$\hat{M}_q = \bigvee_{m_i \in M_P^{\text{filtered}}} m_i. \quad (22)$$

4 Experiments

In our experiments, we evaluate the performance of the proposed MARS on four widely used datasets for FSS: COCO-20ⁱ [17], Pascal-5ⁱ [21, 6], LVIS-92ⁱ [13], and FSS-1000 [10]. We consider both 1-shot and 5-shot scenarios, where one or five support images and their corresponding segmentation masks are provided to guide the segmentation of a query image.

To assess the general applicability of MARS, we selected several state-of-the-art algorithms from the FSS literature to generate mask proposals and coupled them with MARS. Specifically, we combined MARS with **Matcher**, **GF-SAM**, **VRP-SAM**, **PerSAM**, and **SegGPT**—all of which represent the top performers in FSS task.

Segmentation quality is quantified using the mean Intersection Over Union (mIoU) as the evaluation metric, computed following the procedure outlined in [13]. Detailed information about the prompts used for ViP-LLaVA to extract class names and descriptions, the exact specifications of the DinoV2 pre-trained ViT and associated feature maps, as well as the configurations for the ViP-LLaVA, AlphaClip, and CLIP models are provided in the Appendix of the Supplementary Materials. In addition, we adopted the coverage parameter $\alpha = 0.85$ and the values of the static threshold $th_s = 0.55$ and dynamic threshold $th_d = 0.95$ on every experiment.

4.1 Ablation Studies

To evaluate the contribution of each component within the MARS pipeline, we conduct a series of ablation studies on the COCO-20ⁱ dataset. Since our ranking system integrates four distinct types of information—visual, conceptual, local, and global—each forming mutually exclusive pairs, we systematically test all possible configurations. First, we reduce the ranking system to a single component (e.g. *global visual*, *global conceptual*, *local visual*, *local conceptual* scores) to analyze its individual impact. Next, we group components based on broader categories, such as metric scale (global-local) or conceptual relevance (visual-conceptual). All experiments are conducted on COCO-20ⁱ using Matcher as the mask proposal system. Hyperparameters of the pipeline are the ones of the default settings.

Table 1 summarizes the performance of different configurations in terms of mIoU. Notably, combining metrics either by scale (EMD + AlphaClip Score: Global, *RVA* + *VTA*: Local) or by information type (EMD + *RVA*: Visual, AlphaClip Score + *VTA*: Text) leads to significant improvements over using individual metrics alone. This result highlights the complementary nature of the four metrics in assessing the quality of proposed masks. Consequently, it is only through the integration of all four ranking components within MARS that we achieve best results on COCO-20ⁱ.

We also observe that the vision-only ranking system attains the second-highest performance, underlining the dominant role of visual information.

4.2 One-Shot and Five-Shot Segmentation Results

As the core aspect of a FSS pipeline based on a foundational model such as SAM is both the masks’ proposition phase and the subsequent ranking, we further specify the MARS plug-in point for each tested method. For Matcher, we have collected all the unfiltered mask proposals generated after the promptable segmenter module. Similarly, for GF-SAM, we apply our ranking system after the mask generator step and before the point-mask clustering step. The two methods generate many proposals and our ranking system can be tested in a scenario with much possible noise. With PerSAM, as the method proposes a three-steps-cascade-mask-generation refinement, we have collected all proposals produced in each step, for a total number of 9. VRP-SAM is even narrower with its mask proposition, leveraging only one single mask creation based on SAM. We thus chose to force the creation of three masks through SAM API and collect them. These methods prove the effectiveness of MARS even when few options are available.

Last, SegGPT is trained to produce a single prediction for a query image. Thus we developed a query system that leverages three easy data augmentation steps. We apply a random rotation between -30 and +30 degrees, a random horizontal flip, and a random vertical flip, both with 50% probability. We use these pre-processing operations on the query image to retrieve nine different masks

Method	EMD	AlphaClip Score	RVA ranking	VTA ranking	mIoU
Matcher + GV Score	✓				35.2
Matcher + GC Score		✓			38.0
Matcher + LV Score			✓		45.4
Matcher + LC Score				✓	43.3
Matcher + Global Score	✓	✓			41.9
Matcher + Local Score			✓	✓	48.7
Matcher + Conceptual Score		✓		✓	50.0
Matcher + Visual Score	✓		✓		56.0
Matcher + MARS	✓	✓	✓	✓	60.5

Table 1: Ablation studies on the COCO-20ⁱ dataset. Expanding a single score along a specific dimension always lead to improvement. Cooperation between all four scores achieves the best performance, highlighted in bold. Second to best underlined.

from the model, plus the one generated from the original query image. This scenario is exciting, as generating random transformations of the query image could potentially benefit or harm the target mask generation. Nevertheless, thanks to MARS, we can retrieve the correct prediction and even improve overall performance. All other specific hyperparameters are left as in the original work for each method.

Table 2 shows the performance of five state-of-the-art few-shot segmentation methods (PerSAM, VRP-SAM, GF-SAM, Matcher, SegGPT) on the one-shot segmentation task, together with their MARS-refined version. For each method, we downloaded the official code and re-executed or re-evaluated the performances on the datasets (Original column). VRP-SAM scores on LVIS-92ⁱ are missing as the computational requirements for training the model in that scenario are over-demanding.

As shown in Table 2, MARS consistently enhances the performance of all methods and, on most datasets, even surpasses current state-of-the-art scores in 1-shot segmentation. However, for VRP-SAM, the improvement is less significant. We suspect that this is primarily because, for this method, we generate only three mask proposals, which may limit the effectiveness of our ranking system. The only exception is observed on FSS-1000, where our method yields slightly lower scores compared to top-performing models. We hypothesize that this discrepancy is primarily due to the characteristics of the FSS-1000 dataset, which predominantly contains images with large, clearly defined target objects set against simplistic backgrounds. In such oversimplified scenarios, segmentation scores are already near saturation and minor variations in mask predictions can lead to disproportionate fluctuations in the mIoU metric. This limits the benefits of our approach, which is designed to excel in complex scenarios by leveraging subtle multimodal cues.

In Table 3, we report the performance of methods in the 5-shot scenario. The overall performance gain is lower compared to the 1-shot case. Increasing the number of images in the support set refines visual information by enriching the similarity matrix with contributions from five distinct variations of the target object. This improves the model’s ability to generalize based on visual cues. On the other hand, the larger support set offers limited additional

benefits for the conceptual components because the multiple support images are simply summarized within the Textual Information Retrieval module, not contributing to subsequent conceptual stages. Nevertheless, these gains are consistently observed across various mask generation methods and datasets, further validating MARS’s ability to enhance state-of-the-art performance even in the 5-shot scenario. We have reported in the Appendix of the Supplementary Materials several visualizations of the final mask predictions.

4.3 A Simple MARS Pipeline

In this scenario, we assess the autonomous potential of MARS in a single/few-shot segmentation pipeline that relies on minimal prior information. To isolate the effectiveness of our ranking system, we developed a simplified pipeline based on the SAM Automatic Mask Generator (AMG). In this setup, SAM generates mask proposals from a uniform random sampling grid of points, without any guidance regarding the target object. Further information about the SAM mask generation procedure used can be found in the Supplementary Materials. The main motivation of this experiment is to evaluate how well MARS can perform when the quality of mask proposals is deliberately suboptimal, thus removing any bias introduced by advanced FSS-specific proposal methods. This allows us to assess the intrinsic strength of our ranking and merging strategy in handling noisy or imprecise proposals.

Table 4 provides a comparative analysis between the proposed AMG + MARS pipeline and most relevant published methods. Despite the simplicity of the mask proposal stage, our approach has the highest score on COCO-20ⁱ (1-shot) and remains competitive with top-performing methods in other settings. These results underscore the strength of our ranking system, asserting the dominance of the mask selection procedure over the mask proposal stage in FSS.

5 Conclusions and Future Works

In this paper, we presented MARS, a multimodal alignment and ranking system for FSS that overcomes the limitations of relying solely on visual similarity. Our frame-

Table 2: One-Shot Segmentation Results. For each dataset, the table reports the original performance and the performance after applying MARS in terms of mIoU. In each column, we underlined the top performer method for a particular dataset.

Method	COCO-20 ⁱ		Pascal-5 ⁱ		LVIS-92 ⁱ		FSS-1000	
	Original	+ MARS	Original	+ MARS	Original	+ MARS	Original	+ MARS
PerSAM	21.4	28.8 (+7.4)	43.1	56.0 (+12.9)	12.3	13.6 (+1.3)	75.0	79.1 (+4.1)
VRP-SAM	50.1	52.6 (+2.5)	69.2	67.6 (-1.6)	-	-	87.9	86.4 (-1.5)
SegGPT	54.5	59.9 (+5.4)	83.2	84.1 (+0.9)	20.8	24.0 (+3.2)	83.3	84.3 (+1.0)
Matcher	52.7	60.5 (+7.8)	68.1	77.2 (+9.1)	33.0	36.9 (+3.9)	87.0	85.4 (-1.6)
GF-SAM	58.7	61.9 (+3.2)	72.1	75.7 (+3.6)	35.2	38.7 (+3.5)	88.0	87.0 (-1.0)

Table 3: Five-Shot Segmentation Results. For each dataset, the table reports the original performance in terms of mIoU and the performance after applying MARS. In each column, we underlined the top performer method for a particular dataset.

Method	COCO-20 ⁱ		Pascal-5 ⁱ		LVIS-92 ⁱ		FSS-1000	
	Original	+ MARS	Original	+ MARS	Original	+ MARS	Original	+ MARS
SegGPT	61.2	64.3 (+3.1)	86.8	87.8 (+1.0)	22.4	23.5 (+0.9)	86.2	86.3 (+0.1)
Matcher	60.7	63.6 (+2.9)	74.0	80.7 (+6.7)	40.0	40.5 (+0.5)	89.6	87.6 (-2.0)
GF-SAM	66.8	67.8 (+1.0)	82.6	81.5 (-1.1)	44.0	46.7 (+2.7)	88.9	87.5 (-1.4)

Table 4: Performance of well-known methods on one-shot and five-shot segmentation tasks. The table reports mIoU scores. We have highlighted in bold the top performer method and underlined the second-best.

Method	COCO-20 ⁱ		Pascal-5 ⁱ	
	1-shot	5-shot	1-shot	5-shot
HSNet [16]	41.2	49.5	66.2	70.4
VAT [8]	41.3	47.9	67.5	71.6
PerSAM	21.4	-	43.1	-
VRP-SAM	50.1	-	69.2	-
SegGPT	54.5	61.2	83.2	86.8
Matcher	52.7	60.7	68.1	74.0
GF-SAM	<u>58.7</u>	66.8	72.1	<u>82.6</u>
AMG + MARS (Ours)	59.2	<u>64.6</u>	<u>74.3</u>	80.9

Notably, experiments on AMG + MARS, which represent a less optimal proposal generation scenario, validate the strengths of MARS and suggest that it can query a clustering model and transform it from an agnostic segmentation model into a FSS model.

work computes four complementary scores: *Local Conceptual Score (LC)*, *Global Conceptual Score (GC)*, *Local Visual Score (LV)*, and *Global Visual Score (GV)* to evaluate mask proposals. The key innovation lies in the integration of conceptual scores derived from both the class name and a more generic textual description, extracted from resources such as WordNet and via ViP-LLaVA, which serves as a semantic anchor. This multimodal approach effectively mitigates challenges arising from significant visual differences between the support and query images by focusing on the inherent semantic attributes of the object.

Extensive experiments on datasets such as COCO-20ⁱ, Pascal-5ⁱ, LVIS-92ⁱ, and FSS-1000 demonstrate that incorporating MARS into various segmentation methods (including Matcher, GF-SAM, VRP-SAM, PerSAM, and SegGPT) leads to substantial improvements over state of the art performance. Ablation studies further confirm that the fusion of local and global, as well as visual and conceptual information, is essential for robust segmentation.

References

- [1] Mu Cai, Haotian Liu, Siva Karthik Mustikovela, Gregory P. Meyer, Yuning Chai, Dennis Park, and Yong Jae Lee. Vip-llava: Making large multimodal models understand arbitrary visual prompts. In *IEEE/CVF Conference on Computer Vision and Pattern Recognition, CVPR 2024, Seattle, WA, USA, June 16-22, 2024*, pages 12914–12923. IEEE, 2024. [2](#)
- [2] Mathilde Caron, Hugo Touvron, Ishan Misra, Hervé Jégou, Julien Mairal, Piotr Bojanowski, and Armand Joulin. Emerging properties in self-supervised vision transformers. In *2021 IEEE/CVF International Conference on Computer Vision, ICCV 2021, Montreal, QC, Canada, October 10-17, 2021*, pages 9630–9640. IEEE, 2021. [2](#)
- [3] Timothée Darcet, Maxime Oquab, Julien Mairal, and Piotr Bojanowski. Vision transformers need registers. In *The Twelfth International Conference on Learning Representations, ICLR 2024, Vienna, Austria, May 7-11, 2024*. OpenReview.net, 2024. [5](#)
- [4] Nanqing Dong and Eric P. Xing. Few-shot semantic segmentation with prototype learning. In *British Machine Vision Conference 2018, BMVC 2018, Newcastle, UK, September 3-6, 2018*, page 79. BMVA Press, 2018. [2](#)
- [5] Alexey Dosovitskiy, Lucas Beyer, Alexander Kolesnikov, Dirk Weissenborn, Xiaohua Zhai, Thomas Unterthiner, Mostafa Dehghani, Matthias Minderer, Georg Heigold, Sylvain Gelly, Jakob Uszkoreit, and Neil Houlsby. An image is worth 16x16 words: Transformers for image recognition at scale. In *9th International Conference on Learning Representations, ICLR 2021, Virtual Event, Austria, May 3-7, 2021*. OpenReview.net, 2021. [2](#)
- [6] Bharath Hariharan, Pablo Andrés Arbeláez, Ross B. Girshick, and Jitendra Malik. Simultaneous detection and segmentation. In David J. Fleet, Tomás Pajdla, Bernt Schiele, and Tinne Tuytelaars, editors, *Computer Vision - ECCV 2014 - 13th European Conference, Zurich, Switzerland, September 6-12, 2014, Proceedings, Part VII*, volume 8695 of *Lecture Notes in Computer Science*, pages 297–312. Springer, 2014. [6](#)
- [7] Kaiming He, Xiangyu Zhang, Shaoqing Ren, and Jian Sun. Deep residual learning for image recognition. *CoRR*, abs/1512.03385, 2015. [2](#)
- [8] Sunghwan Hong, Seokju Cho, Jisu Nam, Stephen Lin, and Seungryong Kim. Cost aggregation with 4d convolutional swin transformer for few-shot segmentation. In Shai Avidan, Gabriel J. Brostow, Moustapha Cissé, Giovanni Maria Farinella, and Tal Hassner, editors, *Computer Vision - ECCV 2022 - 17th European Conference, Tel Aviv, Israel, October 23-27, 2022, Proceedings, Part XXIX*, volume 13689 of *Lecture Notes in Computer Science*, pages 108–126. Springer, 2022. [2](#), [8](#)
- [9] Alexander Kirillov, Eric Mintun, Nikhila Ravi, Hanzi Mao, Chloe Rolland, Laura Gustafson, Tete Xiao, Spencer Whitehead, Alexander C Berg, Wan-Yen Lo, et al. Segment anything. 2023. [2](#)
- [10] Xiang Li, Tianhan Wei, Yau Pun Chen, Yu-Wing Tai, and Chi-Keung Tang. FSS-1000: A 1000-class dataset for few-shot segmentation. In *2020 IEEE/CVF Conference on Computer Vision and Pattern Recognition, CVPR 2020, Seattle, WA, USA, June 13-19, 2020*, pages 2866–2875. Computer Vision Foundation / IEEE, 2020. [6](#)
- [11] Yuqi Lin, Minghao Chen, Wenxiao Wang, Boxi Wu, Ke Li, Binbin Lin, Haifeng Liu, and Xiaofei He. CLIP is also an efficient segmenter: A text-driven approach for weakly supervised semantic segmentation. In *IEEE/CVF Conference on Computer Vision and Pattern Recognition, CVPR 2023, Vancouver, BC, Canada, June 17-24, 2023*, pages 15305–15314. IEEE, 2023. [4](#)
- [12] Yuqi Lin, Minghao Chen, Wenxiao Wang, Boxi Wu, Ke Li, Binbin Lin, Haifeng Liu, and Xiaofei He. CLIP is also an efficient segmenter: A text-driven approach for weakly supervised semantic segmentation. In *IEEE/CVF Conference on Computer Vision and Pattern Recognition, CVPR 2023, Vancouver, BC, Canada, June 17-24, 2023*, pages 15305–15314. IEEE, 2023. [4](#)
- [13] Yang Liu, Muzhi Zhu, Hengtao Li, Hao Chen, Xinlong Wang, and Chunhua Shen. Matcher: Segment anything with one shot using all-purpose feature matching. In *The Twelfth International Conference on Learning Representations, ICLR 2024, Vienna, Austria, May 7-11, 2024*. OpenReview.net, 2024. [1](#), [2](#), [6](#)
- [14] Yongfei Liu, Xiangyi Zhang, Songyang Zhang, and Xuming He. Part-aware prototype network for few-shot semantic segmentation. In Andrea Vedaldi, Horst Bischof, Thomas Brox, and Jan-Michael Frahm, editors, *Computer Vision - ECCV 2020 - 16th European Conference, Glasgow, UK, August 23-28, 2020, Proceedings, Part IX*, volume 12354 of *Lecture Notes in Computer Science*, pages 142–158. Springer, 2020. [2](#)
- [15] George A. Miller. Wordnet: A lexical database for english. *Commun. ACM*, 38(11):39–41, 1995. [2](#)
- [16] Juhong Min, Dahyun Kang, and Minsu Cho. Hypercorrelation squeeze for few-shot segmentation. *CoRR*, abs/2104.01538, 2021. [2](#), [8](#)
- [17] Khoi Nguyen and Sinisa Todorovic. Feature weighting and boosting for few-shot segmentation. In *2019 IEEE/CVF International Conference on Computer Vision, ICCV 2019, Seoul, Korea (South), October 27 - November 2, 2019*, pages 622–631. IEEE, 2019. [6](#)
- [18] Maxime Oquab, Timothée Darcet, Théo Moutakanni, Huy V. Vo, Marc Szafraniec, Vasil Khalidov, Pierre Fernandez, Daniel Haziza, Francisco Massa, Alaaeldin El-Nouby, Mido Assran, Nicolas Ballas, Wojciech Galuba, Russell Howes, Po-Yao Huang, Shang-Wen Li, Ishan Misra, Michael Rabbat, Vasu Sharma, Gabriel Synnaeve, Hu Xu, Hervé Jégou, Julien Mairal, Patrick Labatut, Armand Joulin, and Piotr Bojanowski. Dinov2: Learning robust visual features without supervision. *Trans. Mach. Learn. Res.*, 2024, 2024. [2](#)
- [19] Alec Radford, Jong Wook Kim, Chris Hallacy, Aditya Ramesh, Gabriel Goh, Sandhini Agarwal, Girish Sastry, Amanda Askell, Pamela Mishkin, Jack Clark, Gretchen Krueger, and Ilya Sutskever. Learning transferable visual models from natural language supervision. In Marina Meila and Tong Zhang, editors, *Proceedings of the 38th International Conference on Machine Learning, ICML 2021, 18-24 July 2021, Virtual Event*, volume 139 of *Proceedings of Machine Learning Research*, pages 8748–8763. PMLR, 2021. [2](#), [4](#), [11](#)
- [20] Kate Rakelly, Evan Shelhamer, Trevor Darrell, Alyosha A. Efros, and Sergey Levine. Conditional networks for few-shot semantic segmentation. In *6th International Conference on Learning Representations, ICLR 2018, Van-*

- cover, BC, Canada, April 30 - May 3, 2018, Workshop Track Proceedings. OpenReview.net, 2018. [1](#)
- [21] Amirreza Shaban, Shray Bansal, Zhen Liu, Irfan Essa, and Byron Boots. One-shot learning for semantic segmentation. In *British Machine Vision Conference 2017, BMVC 2017, London, UK, September 4-7, 2017*. BMVA Press, 2017. [1](#), [6](#)
- [22] Karen Simonyan and Andrew Zisserman. Very deep convolutional networks for large-scale image recognition. In Yoshua Bengio and Yann LeCun, editors, *3rd International Conference on Learning Representations, ICLR 2015, San Diego, CA, USA, May 7-9, 2015, Conference Track Proceedings*, 2015. [2](#)
- [23] Yanpeng Sun, Jiahui Chen, Shan Zhang, Xinyu Zhang, Qiang Chen, Gang Zhang, Errui Ding, Jingdong Wang, and Zechao Li. VRP-SAM: SAM with visual reference prompt. In *IEEE/CVF Conference on Computer Vision and Pattern Recognition, CVPR 2024, Seattle, WA, USA, June 16-22, 2024*, pages 23565–23574. IEEE, 2024. [2](#)
- [24] Zeyi Sun, Ye Fang, Tong Wu, Pan Zhang, Yuhang Zang, Shu Kong, Yuanjun Xiong, Dahua Lin, and Jiaqi Wang. Alpha-clip: A CLIP model focusing on wherever you want. In *IEEE/CVF Conference on Computer Vision and Pattern Recognition, CVPR 2024, Seattle, WA, USA, June 16-22, 2024*, pages 13019–13029. IEEE, 2024. [2](#), [4](#)
- [25] Haochen Wang, Yandan Yang, Xianbin Cao, Xiantong Zhen, Cees Snoek, and Ling Shao. Variational prototype inference for few-shot semantic segmentation. In *IEEE Winter Conference on Applications of Computer Vision, WACV 2021, Waikoloa, HI, USA, January 3-8, 2021*, pages 525–534. IEEE, 2021. [2](#)
- [26] Jin Wang, Bingfeng Zhang, Jian Pang, Honglong Chen, and Weifeng Liu. Rethinking prior information generation with CLIP for few-shot segmentation. In *IEEE/CVF Conference on Computer Vision and Pattern Recognition, CVPR 2024, Seattle, WA, USA, June 16-22, 2024*, pages 3941–3951. IEEE, 2024. [3](#), [4](#), [11](#)
- [27] Xinlong Wang, Xiaosong Zhang, Yue Cao, Wen Wang, Chunhua Shen, and Tiejun Huang. Seggpt: Towards segmenting everything in context. In *IEEE/CVF International Conference on Computer Vision, ICCV 2023, Paris, France, October 1-6, 2023*, pages 1130–1140. IEEE, 2023. [2](#)
- [28] Sergey Zagoruyko and Nikos Komodakis. Wide residual networks. *arXiv preprint arXiv:1605.07146*, 2016. [2](#)
- [29] Anqi Zhang, Guangyu Gao, Jianbo Jiao, Chi Liu, and Yunchao Wei. Bridge the points: Graph-based few-shot segment anything semantically. In Amir Globersons, Lester Mackey, Danielle Belgrave, Angela Fan, Ulrich Paquet, Jakub M. Tomczak, and Cheng Zhang, editors, *Advances in Neural Information Processing Systems 38: Annual Conference on Neural Information Processing Systems 2024, NeurIPS 2024, Vancouver, BC, Canada, December 10 - 15, 2024*, 2024. [1](#), [2](#), [5](#)
- [30] Renrui Zhang, Zhengkai Jiang, Ziyu Guo, Shilin Yan, Junting Pan, Hao Dong, Yu Qiao, Peng Gao, and Hongsheng Li. Personalize segment anything model with one shot. In *The Twelfth International Conference on Learning Representations, ICLR 2024, Vienna, Austria, May 7-11, 2024*. OpenReview.net, 2024. [2](#)
- [31] Xiaolin Zhang, Yunchao Wei, Yi Yang, and Thomas S. Huang. Sg-one: Similarity guidance network for one-shot semantic segmentation. *IEEE Trans. Cybern.*, 50(9):3855–3865, 2020. [2](#)

6 Supplementary Material

These supplemental materials provide additional details and qualitative results to complement the main manuscript.

6.1 Text Prompt For ViP-LLaVa

We retrieve the class name by prompting ViP-LLaVa with the support image and the text prompt:

Prompt 1: ViP-LLaVa Class Name Prompt

```
Human: <image> What is the name of the
  ↪ object inside the red mask
  ↪ contour in the image? Your output
  ↪ must be only the class name of
  ↪ the object. Do not add any
  ↪ additional text.
```

We retrieve the object description of the class name from ViP-LLaVa with the following prompt:

Prompt 2: ViP-LLaVa Class Description Prompt

```
Human: <image> Given the image provided
  ↪ , identify and provide the
  ↪ definition of the {} inside the
  ↪ {} mask contour. Assistant:
```

6.2 Visual Prompt For ViP-LLaVa

We prompt ViP-LLaVa on the support image using a mask contour highlight (red, $\alpha = 0.5$, thickness=2) and a 50% zoom. This configuration is compared with competing ones in Table 5) where we compare three prompt types (mask overlay, bounding box, mask contour), varied contour color, transparency (α), thickness and zoom level, and measuring a configuration accuracy as:

$$\text{Accuracy} = \frac{\#\{\text{matched names}\}}{\#\{\text{total predictions}\}}.$$

Predicted and ground-truth labels are first lowercased and string-compared; only exact matches count as correct. To have a metric more resilient to synonyms, in the column ‘‘Acc. Matching Wordnet Synset(%)’’ we report the Accuracy scores considering a positive match when the prediction and ground truth share the same set of synsets in WordNet; otherwise, they are incorrect.

Zoom-based Cropping. We compute the tightest bounding rectangle around all connected mask components, expand its width and height by the zoom percentage (clipped to image borders), crop, then resize back to the original frame as exemplified in Algorithm 1. When the object already fills most of the image, the result is nearly identical to the original; when the object is small or off-center, the expansion brings it closer into focus so that the vision-language model can attend to it more effectively.

Algorithm 1 Zoom-based Cropping for ViP-LLaVa Prompting

Require: image I , mask M , zoom $Z\%$

Ensure: zoomed crop C

```
1: bbox  $\leftarrow$  get_bbox( $M$ )
2: (bbox.x, bbox.y)  $\leftarrow$  (bbox.xtop-left, bbox.ytop-left)
3: ( $w, h$ )  $\leftarrow$  (bbox.width, bbox.height)
4: bbox.xcenter  $\leftarrow$  bbox.xtop-left +  $w/2$ ,
5: bbox.ycenter  $\leftarrow$  bbox.ytop-left +  $h/2$ 
6:  $w' \leftarrow$  min( $w \times (100/Z)$ ,  $I$ .width)
7:  $h' \leftarrow$  min( $h \times (100/Z)$ ,  $I$ .height)
8: bbox.x'  $\leftarrow$  max(0, bbox.xcenter -  $w'/2$ )
9: bbox.y'  $\leftarrow$  max(0, bbox.ycenter -  $h'/2$ )
10:  $C_{\text{raw}} \leftarrow$  crop( $I$ , bbox)
11:  $C \leftarrow$  resize( $C_{\text{raw}}$ ,  $I$ .width,  $I$ .height)
12: return  $C$ 
```

6.3 Prompt For Visual-Text Alignment Module

The *VTA* serves as a saliency map that highlights the regions in the query image where the object of interest, described by textual information, is likely located. It leverages the visual-textual alignment capabilities of the CLIP model [19].

The construction of *VTA* begins with the class name of the entity of interest extracted by ViP-LLaVa. Two text prompts are then generated: a positive prompt t_{FG}

Prompt 3: ViP-LLaVa t_{FG} Prompt

```
a {predicted_class_name}.
```

and a negative prompt t_{BG} :

Prompt 4: ViP-LLaVa t_{BG} Prompt

```
a photo without {predicted_class_name
  ↪ }.
```

6.4 MARS Default Configuration

The configuration of the models used in MARS and all the experiments is as follows:

- **Text-extraction Module:** this component uses a ViP-LLaVa vision-language model based on LLaVA-7B with 4-bit quantization. The prompting strategies employed to extract relevant information from the support set are detailed in [subsection 6.1](#).
- **Visual-Text Alignment Module:** the proposed method is used to generate *VTA*, computed with a pre-trained CLIP-B/16 model. The threshold parameter in the PIR module, which is applied to refine the initial *VTA*, is set to 0.4 and employs the attention maps extracted from the last 8 self-attention layers (out of the 12) of the encoder, as reported in PI-CLIP [26].
- **Visual-Visual Alignment Module:** this module employs a Vision Transformer ViT-L/14 pre-trained

Table 5: Comparison of visual prompt configurations for class name extraction on COCO-20ⁱ. “Acc. Exact Matching” reports the percentage of predictions that exactly match the ground-truth label; “Acc. Matching Wordnet Synset” reports the percentage of predictions that match via shared WordNet synsets. The best configuration is highlighted in bold.

Prompt Type	Color	Alpha	Thickness	Zoom	Acc. Exact Matching (%)	Acc. Matching Wordnet Synset(%)
mask overlay	red	0.3	1	0	56.37	60.74
bounding box	red	0.5	2	0	62.60	68.29
bounding box	red	0.5	2	30	63.45	69.80
bounding box	red	0.5	2	50	62.82	69.07
mask contour	red	0.5	2	0	62.30	68.75
mask contour	red	0.5	2	30	65.39	71.75
mask contour	green	0.5	2	50	65.70	72.23
mask contour	red	0.5	2	50	65.75	72.25

with DINOv2, specifically the variant using four register tokens, to extract *RVA*. The PIR module threshold used to refine *RVA* is set to 0.85 and employs the attention maps extracted from all 24 self-attention layers of the encoder.

- AlphaClip Module: a pre-trained AlphaCLIP-L/14@336 model is used to compute the global-conceptual score for each mask proposal.
- Filtering-Merging Module: the fixed threshold `static` in the filtering component is set to 0.55. The dynamic threshold `dynamic` is set to 0.95, ensuring that if no proposals exceed the fixed threshold, only those achieving at least 95% of the score of the best proposal are retained.

We have always adopted original weights available from official repositories.

6.5 Computational overhead and resource requirements

We assessed the computational overhead introduced by MARS and found it to be minimal when compared to similar pipelines. In particular, we benchmarked the time required for each component of MARS and the competing method *Matcher* using the COCO-20ⁱ dataset, where hundreds of mask proposals are ranked for a single query. All experiments were run on an NVIDIA Quadro RTX 6000 (24GB), with MARS requiring approximately 18 GB of VRAM to operate.

The initial mask proposal step, performed by SAM, takes approximately 12.1 ± 1.31 seconds, which is consistent across both *Matcher* and MARS. The main distinction lies in the ranking and merging phase. *Matcher* completes this step in 0.27 ± 0.25 seconds, while MARS requires 2.04 ± 0.61 seconds. Despite being slower, this additional cost remains negligible relative to the overall computation time dominated by mask generation.

Additionally, in MARS, class name prediction is required only once per support set. This step takes 4.72 ± 0.59 seconds and is not repeated for subsequent queries referencing the same support set. Therefore, in the typical scenario where the support set has already been processed,

MARS requires approximately 13–14 seconds per prediction, only slightly more than *Matcher*’s 12–13 seconds.

In the worst-case scenario, where the support set is encountered for the first time, the total inference time increases to 18–19 seconds. However, this case occurs only once per novel support set and does not represent the standard operational cost.

6.6 SAM Automatic Mask Generation Hyperparameters

In this section, we report the parameters of the *SamAutomaticMaskGenerator* class (taken from the official *Matcher* repository) used to generate the mask proposals.

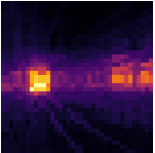
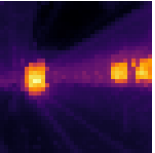
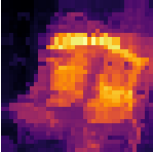
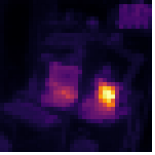
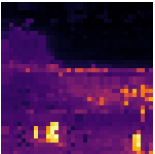
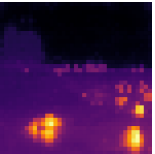
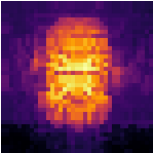
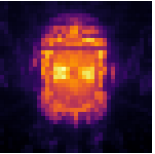
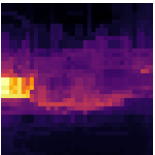
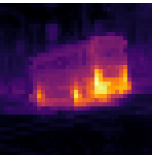
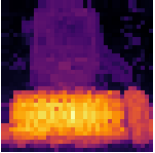
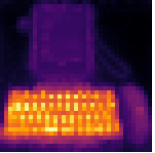
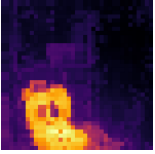
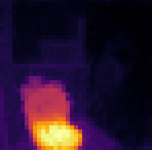
```

points_per_side = 64,
points_per_batch = 64,
pred_iou_thresh = 0.88,
sel_pred_iou_thresh = 0.85,
stability_score_thresh = 0.95,
stability_score_offset = 1.0,
sel_stability_score_thresh = 0.90,
sel_stability_score_offset = 1.0,
box_nms_thresh = 0.65,
crop_n_layers = 1,
crop_nms_thresh = 0.7,
crop_overlap_ratio = 512 / 1500,
crop_n_points_downscale_factor = 2,
point_grids = None,
min_mask_region_area = 14,
output_mode = "binary_mask",
multimask_output = True,
sel_multimask_output = True,
output_layer = -1,
sel_output_layer = -1,
dense_pred = True

```

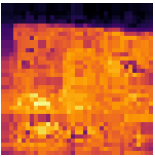
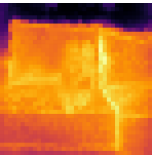
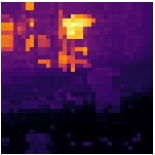
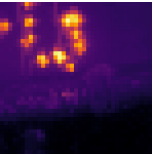
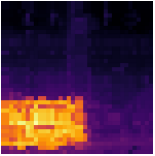
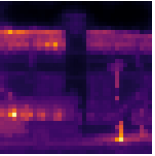
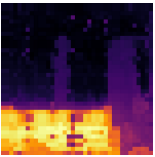
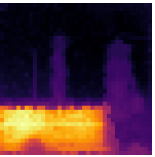
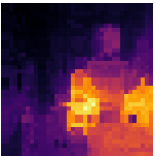
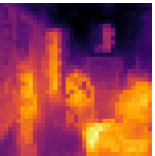
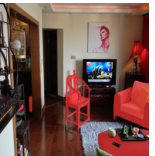
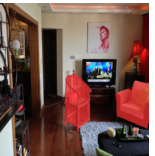
6.7 Qualitative Results

Table 6: **Qualitative Results:** This table presents each sample as a two-part row. The upper part displays the Support Set, Query Image, Visual Prior, Text Prior, Matcher Prediction, Matcher with MARS Prediction, and the Ground Truth. The lower part provides the corresponding textual information: the dataset’s class name, the predicted class name, a description of the subject class inferred by MARS using WordNet, followed by the IoU values for the Matcher prediction and the Matcher with MARS prediction.

Support Set	Query Image	Text Prior	Visual Prior	Matcher	Matcher + MARS	Ground Truth
 train	 Train	 <i>*Description not found*</i>		 7.38 mIoU	 87.11 mIoU	
 tv	 Television	 <i>an electronic device that receives television signals and displays them on a screen</i>		 7.59 mIoU	 86.63 mIoU	
 sheep	 Sheep	 <i>woolly usually horned ruminant mammal related to the goat</i>		 1.67 mIoU	 64.91 mIoU	
 clock	 Clock	 <i>a timepiece that shows the time of day</i>		 2.94 mIoU	 85.34 mIoU	
 car	 Car	 <i>*Description not found*</i>		 1.96 mIoU	 65.84 mIoU	
 keyboard	 Keyboard	 <i>*Description not found*</i>		 12.76 mIoU	 89.25 mIoU	
 toilet	 Toilet	 <i>*Description not found*</i>		 1.96 mIoU	 89.25 mIoU	

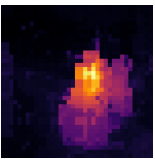
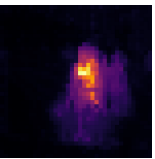
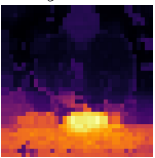
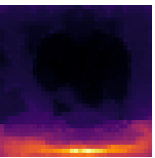
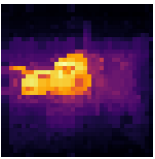
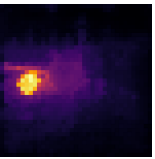
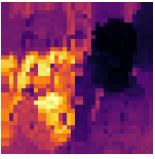
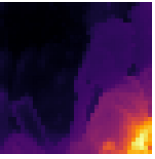
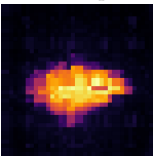
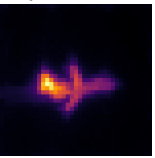
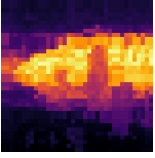
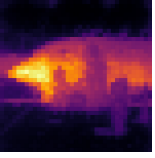
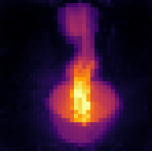
Continued on next page

Table 6 – continued from previous page

Support Set	Query Image	Text Prior	Visual Prior	Matcher	Matcher + MARS	Ground Truth
toilet	Chair	<i>a seat for one person, with a support for the back</i>		0.13 mIoU	38.24 mIoU	
						
couch	Couch	<i>*Description not found*</i>		33.31 mIoU	92.98 mIoU	
						
book	Book	<i>a written work or composition that has been published (printed on pages bound together)</i>		2.47 mIoU	51.30 mIoU	
						
kite	Kite	<i>any of several small graceful hawks of the family Accipitridae having long pointed wings and feed...</i>		0.74 mIoU	59.23 mIoU	
						
bus	Bus	<i>a vehicle carrying many passengers; used for public transport</i>		0.02 mIoU	95.65 mIoU	
						
bench	Bench	<i>the magistrate or judge or judges sitting in court in judicial capacity to compose the court coll...</i>		0.00 mIoU	94.98 mIoU	
						
chair	Seat	<i>any support where you can sit (especially the part of a chair or bench etc. on which you sit)</i>		0.00 mIoU	57.79 mIoU	

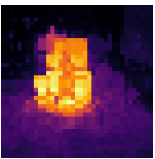
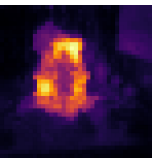
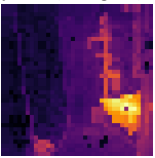
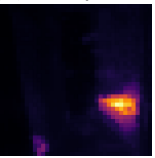
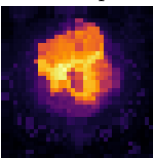
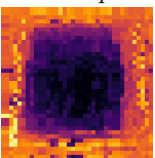
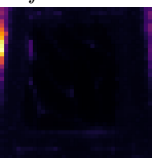
Continued on next page

Table 6 – continued from previous page

Support Set	Query Image	Text Prior	Visual Prior	Matcher	Matcher + MARS	Ground Truth
						
backpack	Backpack	<i>a bag carried by a strap on your back or shoulder</i>		0.00 mIoU	58.18 mIoU	
						
dining table	Table	<i>a company of people assembled at a table for a meal or game</i>		19.90 mIoU	58.23 mIoU	
						
airplane	Airplane	<i>an aircraft that has a fixed wing and is powered by propellers or jets</i>		10.36 mIoU	72.47 mIoU	
						
chair	Chair	<i>*Description not found*</i>		0.17 mIoU	40.51 mIoU	
						
airplane	Jet engine	<i>a gas turbine produces a stream of hot gas that propels a jet plane by reaction propulsion</i>		0.12 mIoU	83.25 mIoU	
						
airplane	Airplane	<i>an aircraft that has a fixed wing and is powered by propellers or jets</i>		35.28 mIoU	91.19 mIoU	
						
toothbrush	Toothbrush	<i>small brush; has long handle; used to clean teeth</i>		23.30 mIoU	59.88 mIoU	

Continued on next page

Table 6 – continued from previous page

Support Set	Query Image	Text Prior	Visual Prior	Matcher	Matcher + MARS	Ground Truth
 cake	 Cake	 <i>baked goods made from or based on a mixture of flour, sugar, eggs, and fat</i>		 0.87 mIoU	 74.98 mIoU	
 sink	 Sink	 <i>*Description not found*</i>		 5.07 mIoU	 94.34 mIoU	
 cake	 Cake	 <i>*Description not found*</i>		 8.21 mIoU	 73.46 mIoU	
 truck	 Truck	 <i>an automotive vehicle suitable for hauling</i>		 1.51 mIoU	 75.79 mIoU	